The Motion Suspension System for On-Ground Tests of Space Robots: Demonstration and Results

Ferdinand Elhardt, Marco De Stefano, Manfred Schedl, Martin Stelzer, Andreas Stemmer, Ismael Rodriguez, Ria Vijayan, Máximo A. Roa
Institute of Robotics and Mechatronics
German Aerospace Center, DLR
Muenchener Str. 20
82234 Oberpfaffenhofen, Germany
ferdinand.elhardt@dlr.de

Tobias Bruckmann
Chair of Mechatronics
University of Duisburg-Essen
47048 Duisburg, Germany

***Abstract*—Space robotics plays a significant role in advancing space exploration creating various opportunities for upcoming space missions. Robotic systems deployed on satellites can be used to extend the lifetime of target satellites, inspect orbital assets, and support the deorbiting process. On-ground verification and validation are essential for ensuring the reliable performance of the robot in space. However, space robots are designed for zero gravity conditions, but are tested within Earth's gravity. This creates significant challenges as the robotic joints provide limited torque preventing them from performing movements in Earth's environment. Against this background, the Institute of Robotics and Mechatronics at the German Aerospace Center (DLR) and the University of Duisburg-Essen have developed the Motion Suspension System (MSS), a cable-driven parallel robot that enables space robots to operate in the full three-dimensional workspace. This paper outlines initial experiences with the MSS by focusing on a contact-oriented task utilizing the space-qualified DLR robot arm CAESAR (Compliant Assistance and Exploration SpAce Robot). It shows the applied suspension forces of the MSS in relation to the robot arm's gravitational force, discusses the system's limitations and capabilities in executing complex trajectories, and presents general lessons learned from using the MSS for verification.**

TABLE OF CONTENTS

1. INTRODUCTION

Space robotics plays a crucial role in the domain of space exploration and creates numerous opportunities for future space missions [1]. Free-flying robots mounted on satellites or space stations pave the way for manifold possibilities in future space missions including satellite lifetime extensions, orbital asset inspections, and deorbiting [2]. Since 2001, the Canadarm2 [2] has been a successful space robot that has helped with docking maneuvers, assembly, and maintenance on the International Space Station.

Given its relevance, the verification and validation of space robots and their components is crucial. Once they have been deployed, maintenance becomes a difficult and mostly impossible task. Thus, realistic on-ground tests of the robotic system are important to ensure the robot's reliable performance [3]. However, on-ground tests of space robots pose a significant challenge: space robots are designed to operate in zero gravity, but are tested under the influence of Earth's gravity. Above this, serial space robots are limited in the torque necessary to move on ground, i.e., they cannot withstand their weight in Earth's gravity [1].

Most test facilities [4] for non-gravity-bearing space robots are based on planar air bearings [5]–[7], helium balloons [8], neutral buoyancy [9], free-fall/parabolic flights [10]–[13], and rail-based suspension systems [1], [14]. Air bearings [5]–[7] is the most commonly used concept in space mechanism test facilities, for example, the *Orbital Robotics Lab* at *ESA ESTEC* [15]. The space asset is placed on several platforms that create a thin layer of air between the platform and the floor. This allows for nearly frictionless movement, limited only by the accuracy of the flatness of the floor [15]. However, this method alters the dynamics of the space robot [16] and is limited to horizontal movements. This presents a significant drawback when performing complex tasks such as grasping, vision-based approaches, or FDIR trajectories as these require the robot's full three-dimensional workspace. Helium balloons [8] employ the uplifting force of helium in the air to support space structures. They are commonly used to support large structural elements such as solar sails and solar arrays when deploying them during on-ground tests [17]. Helium balloons are usually large and feature high inertia [18]. Neutral buoyancy [9] uses the uplifting force of objects in water to compensate for gravitational force, resulting in a close approximation of zero gravity. This is often used for astronaut training and can be adapted to test space robots [19]. However, neutral buoyancy is strongly affected by hydrodynamic effects which leads to damping [4]. Free-fall/parabolic flights provide $20\,\mathrm{s}$ of nearly zero gravity using a refitted aircraft performing a parabolic path [10], [11]. Drop towers [12], [13] form an alternative to parabolic flights and provide $4\,\mathrm{s}$ of less than 10^{-6} g. Rail-based suspension systems [20], [21] are usually designed as Gantry cranes with passive [20], [21], or active [22] force compensation. Mechanical suspension systems are often more flexible in positioning. However, the heavy structure leads to low mechanical modes and strong friction effects [23].

To mitigate these drawbacks, the *Institute of Robotics and Mechatronics* at DLR and the *Chair of Mechatronics* at the *University of Duisburg-Essen* have developed the MSS [24], as shown in Figure 1. The MSS is a cable-driven parallel

979-8-3503-0462-6/24/$31.00 ©2024 IEEE
[2] www.asc-csa.gc.ca/eng/iss/canadarm2

robot that meets the necessary requirements for a space robot suspension system [25]. Cable-driven parallel robots are known for their low influence on dynamics and find applications in various fields such as automated construction [26]–[28], logistics [29], [30], or human rehabilitation [31]. These robots consist of cables connected to a mobile platform with multiple degrees of freedom and coiled around motorized cable drums. The cables are guided by pulleys to maneuver the platform within the workspace. Cable-driven parallel robots have characteristics such as lightweight design, large workspace, and exceptional dynamics [32]. This makes them well suited for a space robot suspension system. De Stefano *et al.* [33] have developed a suitable algorithm that enables the computation of suspension forces by formulating an optimization problem designed to minimize the joint torques of the space robot.

This paper presents the first demonstration and results of using the MSS with the space robot CAESAR [34] by DLR. It contributes to the community by providing lessons learned regarding the use of the MSS and presenting measurements of its performance for analysis and further approaches. The paper is structured as follows: first, it describes the setup including the involved components. Then it describes the experimental validation using the MSS in a contact-oriented task. The fourth section presents force/torque and positional measurements forming the basis of the following discussion section. Additionally, it covers general lessons learned with the MSS. The conclusion evaluates the findings and contextualizes them on a broader scale.

2. Setup of Space Robot and MSS

The setup is shown in Figure 1 and comprises the MSS [24], the space robot CAESAR [34], and an Orbital Replacement Unit (ORU). The ORU has a Standard Interface, the Hotdock

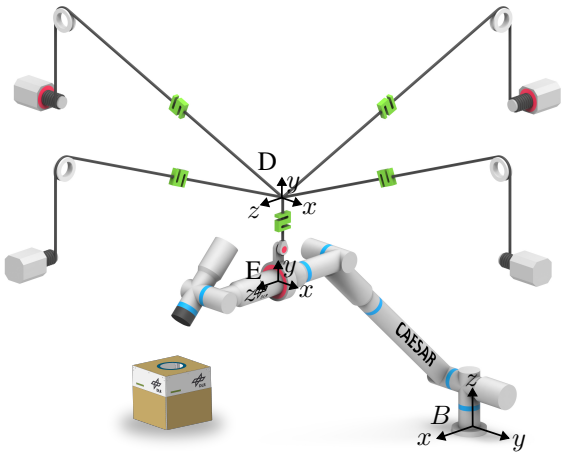

Figure 1. The MSS suspends a space robot arm (here CAESAR) and allows it to move in a large three-dimensional workspace. The cable force sensors are illustrated in green.

[35], and can be latched with a corresponding Standard Interface located at the CAESAR robot end-effector. The space robot is rigidly mounted on the floor and has a working radius of 2.5 m. The MSS is connected to the space robot. The following section provides a detailed description of the setup and its components.

CAESAR

The space-qualified robot arm CAESAR [34] shown in Figure 2 is used in this setup. It is specifically designed

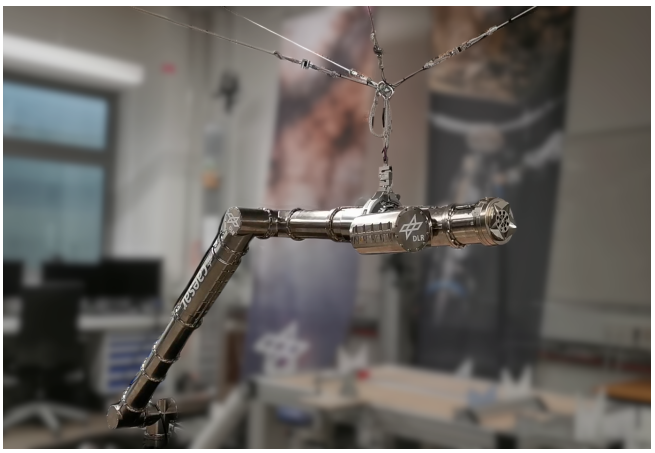

Figure 2. CAESAR (Compliant Assistance and Exploration SpAce Robot) developed by the Institute of Robotics and Mechatronics at the German Aerospace Center (DLR).

for on-orbit operations, including repairing, refueling, and assembly. CAESAR has $n = 7$ joints, each equipped with torque sensors that enable position and impedance control. The impedance control mode allows the robot arm to safely perform contact-oriented tasks while continuously measuring the forces in each joint. The joints and the Robot Control Unit (RCU) are connected using the *EtherCAT* real-time communication bus. The robot arm weights approximately 60 kg and has an adaptable length of 2.5 m. As it is non-gravity-bearing, an external support system, such as the MSS, is necessary to operate on ground.

Dynamics of a Fixed-Base Manipulator in Zero Gravity—We consider that the platform where the manipulator is mounted is large enough such that the arm motion has marginal influence on the base. As such, the dynamics of a general, fixed-base robotic manipulator in zero gravity is defined as

$$\boldsymbol{M}(\boldsymbol{q})\ddot{\boldsymbol{q}} + \boldsymbol{C}(\boldsymbol{q}, \dot{\boldsymbol{q}})\dot{\boldsymbol{q}} = \boldsymbol{\tau}_c \tag{1}$$

where $\boldsymbol{q} \in R^n$ are the joint angle positions of the space robot, $\dot{\boldsymbol{q}} \in R^n$ and $\ddot{\boldsymbol{q}} \in R^n$ are its velocity and acceleration, respectively. The mass matrix is described by $\boldsymbol{M} \in R^{n\times n}$ and the Coriolis matrix by $\boldsymbol{C} \in R^{n\times n}$. The torque of the space robot to perform the maneuvers in space is denoted by $\boldsymbol{\tau}_c \in R^n$. Note the absence of any gravitational influence. We also neglect the influence of orbital dynamics.

Dynamics of a Manipulator on Ground— When operating the space robot on ground with the support of the MSS, the gravitational torque $\boldsymbol{g} \in R^n$ and the acting wrench $\boldsymbol{\Gamma}_c = \boldsymbol{B}^T {}_B\boldsymbol{f}_C$ of the MSS need to be considered. Hereby, $\boldsymbol{B}^T \in R^{6\times 3}$ maps the three-dimensional[3] suspension force ${}_B\boldsymbol{f}_C \in R^3$ onto the entire wrench space $\boldsymbol{\Gamma}_c \in R^6$ of the robot. The robot dynamics is then

$$\boldsymbol{M}(\boldsymbol{q})\ddot{\boldsymbol{q}} + \boldsymbol{C}(\boldsymbol{q}, \dot{\boldsymbol{q}})\dot{\boldsymbol{q}} + \boldsymbol{g}(\boldsymbol{q}) = \boldsymbol{\tau}_c + \boldsymbol{\tau}_g + \boldsymbol{J}_C^T(\boldsymbol{q})\boldsymbol{\Gamma}_c \tag{2}$$

[3] three translational degrees of freedom without rotation

with the Jacobian matrix $\boldsymbol{J}_C^T \in R^{6\times n}$ transforming the suspension wrench $\boldsymbol{\Gamma}_c$ into the joint torque space. The vector $\boldsymbol{\tau}_g \in R^n$ contains the additional torques necessary to compensate for gravity on the robot side.

Note that the MSS can only support joints that are located between the MSS and the robot base in the robot's kinematic chain. We define the joint set A affected by the support and the joint set B unaffected by the support of the MSS. We can split the gravity vector as

$$\boldsymbol{g} = \begin{bmatrix} \boldsymbol{g}_A \\ \boldsymbol{g}_B \end{bmatrix} . \tag{3}$$

The Motion Suspension System

The MSS [24], shown in Figure 1, is a cable-driven parallel robot used as a support facility for on-ground test of space robot arms. The MSS is attached to the space robot at point E and applies an uplift suspension force ${}_B\boldsymbol{f}_C$ (defined in the base frame B on the space robot) that reduces the primarily gravitational torque loads in the space robot's joints. Four actuated direct-drive motors allow the execution of complex three-dimensional trajectories and create the force to support the space robot in Earth's gravity. The cascaded control system [24] is a combination of a PD controller and an admittance controller, which regulates the suspension force at the connection point of the space robot.

The position of the MSS's end effector is determined by the location of frame D (see Figure 1) and measured using the forward kinematics of the MSS and the cable lengths. The method for reconstructing the effective suspension force includes measurements from two angle sensors at the coupling mechanism (point E) and kinematic information from the space robot. The strategy for computing the desired suspension force is presented by De Stefano *et al.* [33] and is based on the dynamics matching of the zero-gravity (Equation 1) and on-ground robot dynamics (Equation 2). The equality constraints in Equation 4 can be obtained by subtracting Equation 2 from 1 and applied to the controllable robot joints in set A, see [3], [33] for details. This forms the basis of the optimization problem which aims to reduce the space robot's joint torques and it is reported as follows,

$$\begin{aligned} \min_{(\boldsymbol{\tau}_{\boldsymbol{gA}},\ {}_B\boldsymbol{f}_C)} \quad & \frac{1}{2}\begin{bmatrix} \boldsymbol{\tau}_{gA}^T & {}_B\boldsymbol{f}_C{}^T \end{bmatrix} \begin{bmatrix} \boldsymbol{W}_{\boldsymbol{\tau}} & \boldsymbol{0} \\ \boldsymbol{0} & \boldsymbol{W}_{\boldsymbol{f}} \end{bmatrix} \begin{bmatrix} \boldsymbol{\tau}_{gA} \\ {}_B\boldsymbol{f}_C \end{bmatrix} \\ \text{s.t. } & \boldsymbol{g}_A = \boldsymbol{\tau}_{gA} + \boldsymbol{J}_{cA}^T\, {}_B\boldsymbol{f}_C \end{aligned} \tag{4}$$

where $\boldsymbol{\tau}_{gA}$ is the gravity torque component of the influenceable set A of joints in the space robot. $\boldsymbol{W}_{\boldsymbol{\tau}} \in R^{3\times3}$ and $\boldsymbol{W}_{\boldsymbol{f}} \in R^{3\times3}$ are the weighting matrices and $\boldsymbol{J}_{cA}$ is the Jacobian matrix at the coupling frame E. The result of the above problem satisfies the equality constraint ensuring full gravity compensation of the space robot, see [33].

Standard Robotic Interface

We use the Hotdock [35] developed by *Space Application Services* as the standard robotic interface for connecting the space robot to the ORU. The Hotdock provides mechanical connection, power, and data transfer. Because of the mating mechanism, it can compensate for positional inaccuracies during latching.

Orbital Replacement Unit (ORU)

An ORU is a self-contained box based on a modular satellite design philosophy that allows for easy replacement of satellites components. The concept of an ORU was first used in the Hubble telescope [36]. The ORU used in our experiment is equipped with two Standard Connectors on two opposite sides. This allows the ORU to be connected to existing satellite structures and extend its functionality. We use a mock-up ORU in our experiment to demonstrate latching and displacement.

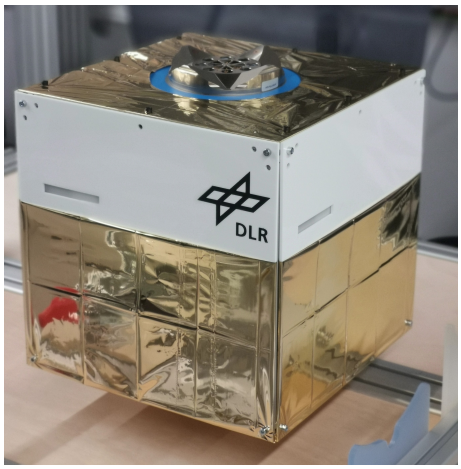

Figure 3. The ORU is a $30\,\mathrm{cm}$ x $30\,\mathrm{cm}$ x $30\,\mathrm{cm}$ box of $6.8\,\mathrm{kg}$ that can contain space components for replacement. This mockup ORU is empty except for a signal LED indicating power.

3. CONTACT-DRIVEN EXPERIMENTAL VALIDATION

The experiment presented in this work aims to analyze a contact-oriented task taking into account the relevant components, which include the MSS, the space robot, and the ORU. Its goal is to collect measurements which can be used for validating system requirements. In the initial state, the upper Standard Interface on the ORU is connected to the space robot as a payload. It hovers above the placement table and the MSS is attached to the space robot. In the final configuration, the ORU is on the placement table and the CAESAR robot arm is disconnected from the ORU, as shown in Figure 4.

The complete task is divided into a series of sequential steps, as shown in Figure 5. The process begins with the *Approaching (1)* phase, during which the robot arm lowers the ORU to its placement table. During this phase, the robot arm is controlled in position mode. The system then moves to the *Contact (2)* phase, where the space robot arm operates in impedance mode, allowing it to response to contact dynamics. It continues to lower the ORU until the lower Standard Interface contacts the corresponding connector on the placement table. In doing so, the impedance mode provides a soft stiffness to the space robot's end effector, resulting in an adaptive glide into the Standard Interface.

Once the contact is established, the system performs a *Payload Adjustment (3)* step in which the ORU mass is subtracted from the considered total robot mass to ensure precise handling and balance. During the subsequent *ORU Decoupling (4)* phase, the Standard Interface opens and disconnects the space robot from the ORU. This is followed by the *Separation (5)* phase. Finally, the system proceeds to the

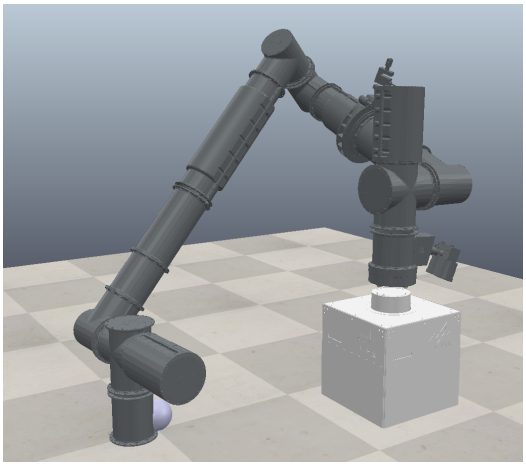

Figure 4. Simulation of the experiment for visualization.

Retreating (6) phase, where the space robot moves away from the ORU in preparation for possible subsequent tasks.

4. RESULTS

The results include measurements based on the experiment presented in the previous section. They are shown in Figure 6. The upper graph shows the position of the MSS at frame D (see Figure 1) and the suspension force between the MSS and the space robot. The trajectory shown is mainly characterized by movement in the z direction, so only the z coordinates of the measurements are shown. The lower graph focuses on the space robot and illustrates the joint angles and joint torques. We show joint 2 and 3 because they are the most loaded joints and are representative of the other joints. The torque is measured directly and combines $\boldsymbol{\tau}_c$, $\boldsymbol{\tau}_g$, and control error. Note that the angle and torque direction of joint 2 and 3 are set so that the robot's end effector moves and pushes *down* with *higher* angle values.

The measurement includes the phases *Approaching (1)*, *Contact (2)*, *Payload Adjustment (3)*, *ORU Decoupling (4)*, *Separation (5)*, and *Retreating (6)*. The initial z position of the MSS (frame D in Figure 1) is $1.87\,\mathrm{m}$ above the ground. The suspension force in the z direction is $360\,\mathrm{N}$, and the torque of the second joint is $15\,\mathrm{N\,m}$. During the *Approaching (1)* phase, the MSS end effector lowers by $0.12\,\mathrm{m}$, while the z-axis suspension force continuously adapts to the space robot's kinematic configuration. The angle of joint 2 and 3 adapt accordingly. The *Contact (2)* between the ORU and the table results in a small oscillation of the z suspension force when the lowest possible z-position is reached. The robot increases the pressure force to ensure a firm contact, which is indicated by an increase in the torque of joint 2 and 3. The impedance controller of the CAESAR robot arm allows it to interact dynamically in this contact-oriented task, compensating for positional uncertainties through small horizontal movements while sliding in the corresponding HOTDOCK shape. Figure 7 shows the position and angle of the tool center point (TCP) during the *Contact* phase. Note that z is pointing down.

To hold the position, the robot returns to *Position Mode*. The *Payload Adjustment (3)* is performed to remove the mass of the ORU from the total mass of the robot in order to prepare the space robot's kinematic calculation for further operation without payload. The graph shows the decreasing load in the suspension force ($350\,\mathrm{N}$ to $290\,\mathrm{N}$) and in the torque of 2nd joint ($24\,\mathrm{N\,m}$ to $12\,\mathrm{N\,m}$).

The *ORU Decoupling (4)* phase shows no movement, but the suspension force reacts with a small oscillation with an amplitude of $1.7\,\mathrm{N}$. During *Separation (5)*, the space robot switches to impedance mode. This controller transition results in small oscillations with an amplitude of $4\,\mathrm{N}$ on the suspension force and an increased torque in the second joint. During the *Retreating (6)* phase, the space robot moves up $15\,\mathrm{cm}$ while the suspension force and the joint torque continuously adapt to the kinematic configuration of the space robot.

The required joint torque depends on the suspension force of the MSS. Figure 8 shows a simulation-based comparison of the same trajectory without the MSS. The simulation was performed in *Mathworks Matlab Simulink* and includes the kinematics and dynamics parameters of the space robot arm. Note that for simplicity, the ORU payload mass was considered attached to the robotic arm for the entire trajectory.

5. DISCUSSION

Elhardt *et al.* [25] describe the system requirements for a space robot suspension system and present a first conceptualization. The requirements cover the ability for gravity compensation, geometric flexibility, ability for dynamics analysis, and usability. The system design based on the requirements is presented by Elhardt *et al.* [24]. In this section, the first experiences with the MSS as a tool for the development and qualification of a space robot arm, such as CAESAR, are discussed with reference to the stated system requirements. This follows a requirement validation approach.

The primary objective of the MSS is to minimize the joint loads of a space robot arm during on-ground experiments [25]. To demonstrate this, we compare the experimental measurements with a simulated, unsupported approach of the same trajectory shown in Figure 8. In this simulation without the MSS, the required absolute joint loads of the same trajectory are in the range of $95\,\mathrm{N\,m}$ to $300\,\mathrm{N\,m}$ for joints 2 and 3. This is clearly above the maximum allowable joint torque of $80\,\mathrm{N\,m}$ [34]. For comparison, the torque loads *with* the support of the MSS during the experiment are in the range of $0\,\mathrm{N\,m}$ to $30\,\mathrm{N\,m}$, see the lower graph in Figure 6 and Figure 8. This is within the allowable joint torque. Note that the joints considered are part of set A and are therefore affected by the suspension force (see Equation 3). This shows that the MSS reduces the joint loads by up to $90\,\%$ for this trajectory. The remaining load is distributed by the gravity compensation strategy to the gravity compensation torque $\boldsymbol{\tau}_g$ of the space robot, especially the joints in set B that need to fully compensate the gravity.

The gravity compensation strategy (see Equation 4) also considers the attached payload in the gravity term $\boldsymbol{g}_A$. According to Equation 2, this is compensated by the MSS wrench $\boldsymbol{\Gamma}_c$ and the gravity compensation torque $\boldsymbol{\tau}_g$. This can be observed during the *Payload Adjustment (3)* phase in Figure 6, as the strategy turns off the payload consideration here. It shows that the suspension force decreases by $60\,\mathrm{N}$ from $350\,\mathrm{N}$ to $290\,\mathrm{N}$. This results in a force of approximately $66\,\mathrm{N}$ at the CAESAR's end effector which covers $95\,\%$ of the ORU's mass ($6.9\,\mathrm{kg}$). The remaining mass is covered by the gravity compensation torque $\boldsymbol{\tau}_g$ of the space robot's joints.

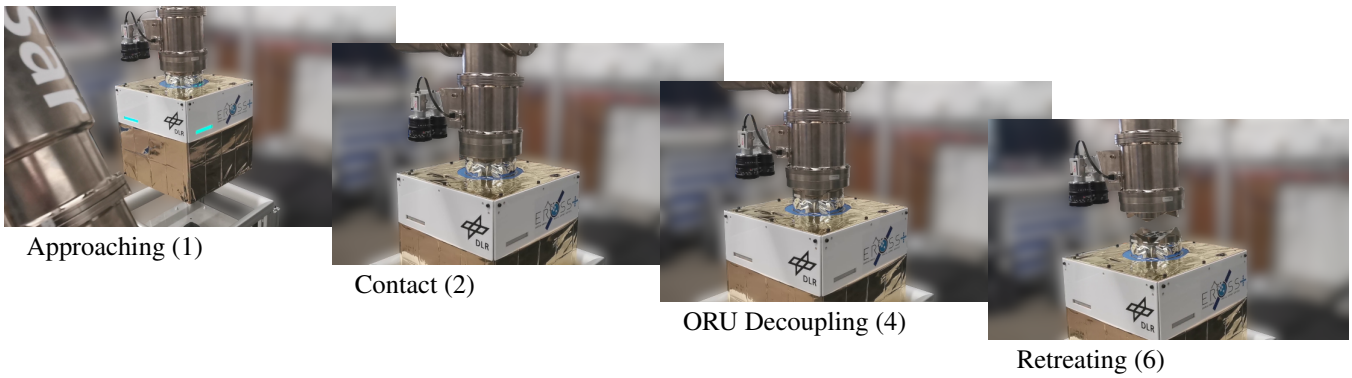

Figure 5. The contact-oriented maneuver starts with an *approach* phase with the ORU latched. The space robot places the ORU on the placement table and disengages. After *retreating*, the space robot is ready to perform the next task.

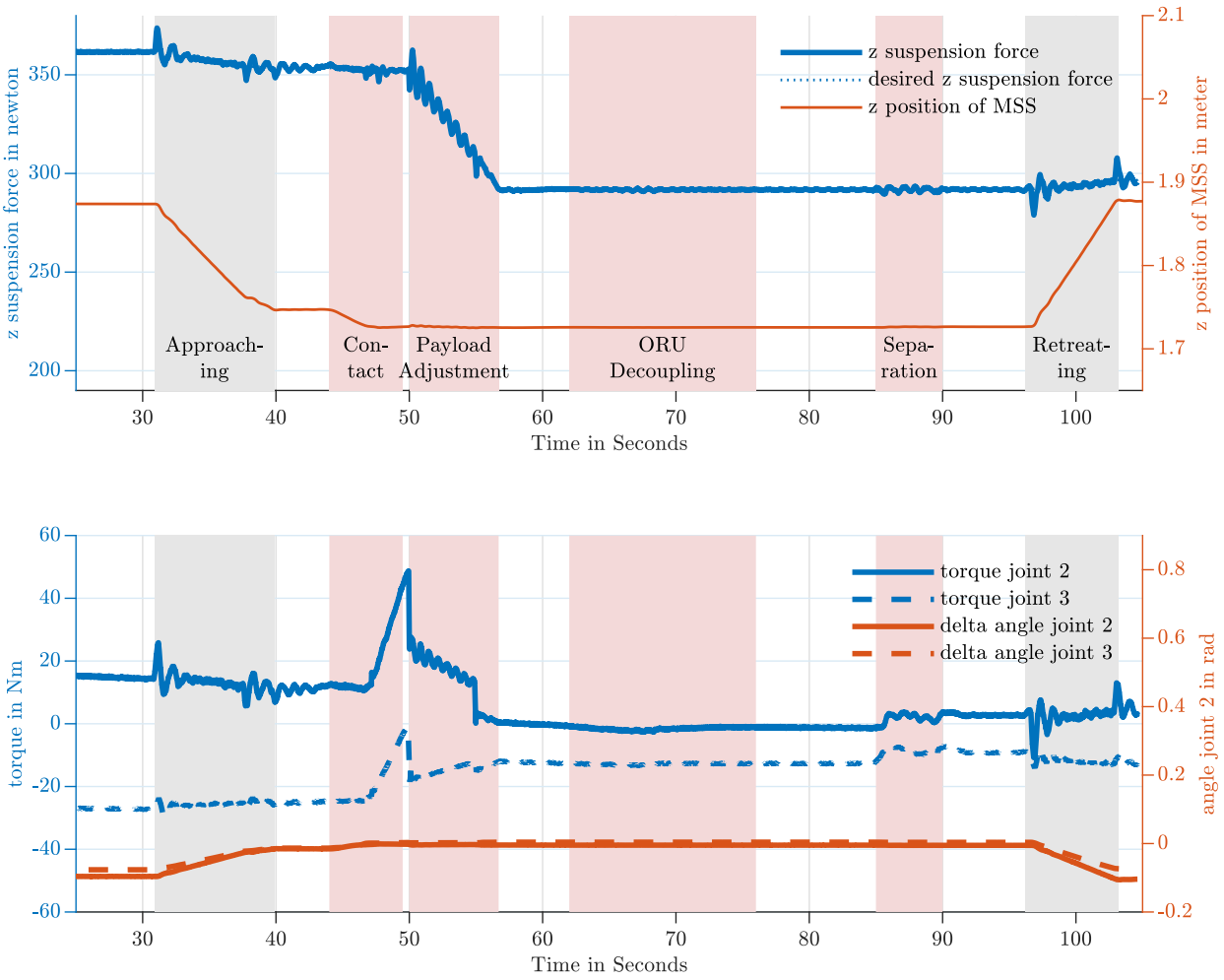

Figure 6. The upper graph shows the suspension force and position of the MSS in z direction. The lower graph illustrates the space robot's motion with joint 2 and 3 as representatives. The colored areas describe the phase during the task.

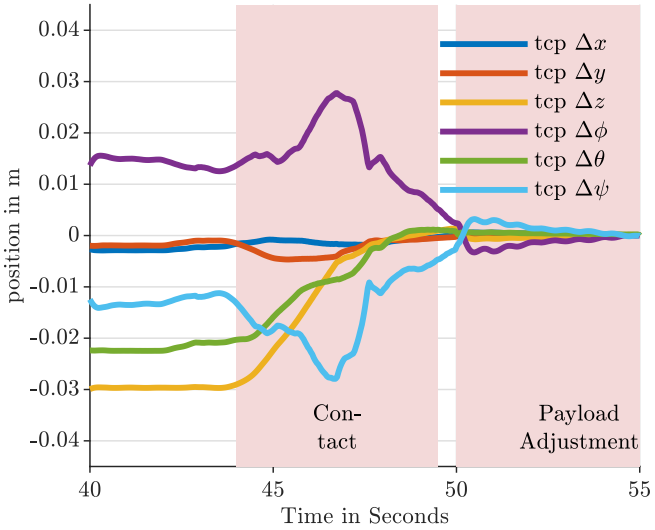

Figure 7. The position and angles of the CAESAR's end effector during the *contact* phase shows small adjustments for position compensation. Note that positive z points down and offsets are used for scaling.

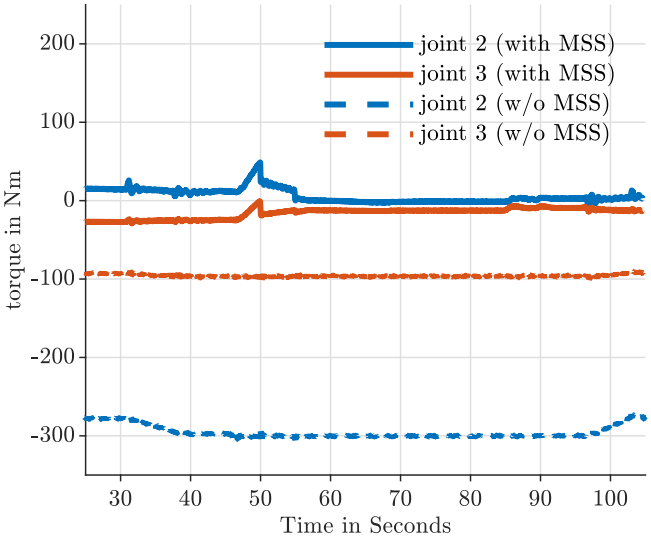

Figure 8. The torque of the robot joints compared with (experiment) and without (simulation) the support of the MSS. The ORU payload mass is considered for the whole trajectory.

However, the support provided by the MSS is limited to the joints in set A, which are located between the CAESAR's mounting point and the robot base. As a consequence, the maximum payload mass is limited because the remaining joints are unsupported. As a result, on-ground tests for on-orbit scenarios with representative high-mass client satellites are not feasible due to the resulting high gravitational forces. In this case, a hardware-in-the-loop method can be used to simulate a floating satellite, as done by De Stefano *et al.* [37].

Complex trajectories such as vision-based maneuvers or grasping trajectories require the robot's end effector to move in all six degrees of freedom. These motions must be supported by the MSS, as formulated requirement for a space robot suspension system [25]. In the experiment shown, the latching of the ORU on the resting table requires that the two contact planes in the standard interface are precisely connected to allow data transfer. The shape of the HOTDOCK interface allows both parts to slide to reach the mating position to overcome positional uncertainties in the robot arm. This requires a spring-like impedance behavior of the space robot arm to interact with the environment and to respond to contact forces. Figure 7 shows the small corrective motions of the robot arm during the latching process at $t = 45\,\mathrm{s}$. It shows that the MSS allows these movements. It also follows the motions of the space robot in performing the small adjustment motions in all directions during latching.

Using the MSS alone does not create a zero-gravity environment. Only in combination with the gravity compensation strategy (Equation 4) are the additional gravity compensation torques for the robot joints computed and executed. Thus, the measured joint torque is the sum of the gravity compensation torque $\boldsymbol{\tau}_g$, the zero-gravity motion torque $\boldsymbol{\tau}_c$ and the residual error. The residual error depends on the accuracy of the robot kinematics and dynamics model, the measurement methods, unaccounted acceleration forces and other factors.

The shown method assumes a fixed-base robot. This assumption holds if the platform is much heavier than the robot arm. If lighter platforms are considered, the coupled dynamics between the arm and the platform needs to be taken into account by applying the methodology described by Mishra *et al.* [38].

From a practical standpoint of handling and usability, the MSS has shown great advantages with minimal modification required for the integration in the space robot. The coupling mechanism can be easily removed without leaving any mechanical residue making it suitable for testing with flight or protoflight models. In addition, the duration of the experiment is unlimited which is in contrast to air bearings (the mobile air tank has to be refilled) and parabolic flights (only a few seconds of zero gravity). Based on our experience, this factor plays an important role in software testing and greatly accelerates the development process compared to support systems with limited experiment duration.

The MSS is not mobile due to its fixed mounting structure within the laboratory environment. As a result, moving the MSS to alternative locations, such as clean rooms or integration sites, becomes a challenging endeavor. In contrast, a helium balloon offers much greater flexibility because it is independent of any infrastructure, except of its huge spatial dimensions. On the contrary, the MSS is characterized by its compactness compared to air-bearing setups or free-fall towers. Based on our experience during several tests, the entire MSS setup imposes minimal interference on other test equipment as it occupies only the upper level space of the room. This advantageous feature ensures that the floor remains unobstructed for the experimental setup.

6. Conclusion

This paper shows the MSS in its first application with the space robot CAESAR and presents the lessons learned from their use as a qualification device. A contact-oriented maneuver was demonstrated. The results present relevant measurements of suspension force, robot end effector position, and

robot joint torques, allowing further investigation of contact dynamics. The discussion section delves into lessons learned from using the system during the development process of the CAESAR space robotic arm.

Many advantages are worth highlighting, including the performance of the suspension capability, the ability to move in all six degrees of freedom and the unlimited test duration. Other test approaches may be more advantageous in terms of providing zero gravity such as underwater buoyancy tests, but require highly invasive modifications to the robot to make it waterproof. In addition, the gravity compensation components are measurable and consists of the combination of the MSS suspension force and the gravity compensation torque. The limitation of the system is its limited payload capacity due to unsupported robot joints. In conclusion, the MSS shows great performance and flexibility for development and qualification testing.

Looking ahead, further improvements can be made the MSS controller to reduce unwanted oscillations. This will require a more sophisticated model of the cables. To increase usability, improvements in the state machine are planned to better integrate the MSS into the space robot's workflow. Optical motion tracking systems can help to provide a ground truth of the position data, such as the position of the MSS or the space robot, to evaluate deviations. A comparative analysis with other suspension systems can be performed.

REFERENCES

[1] E. Papadopoulos, F. Aghili, O. Ma, and R. Lampariello, "Robotic Manipulation and Capture in Space: A Survey," *Frontiers in Robotics and AI*, 2021. DOI: 10.3389/frobt.2021.686723.

[2] R. H. Miller, M. L. Minsky, and D. B. S. Smith, "Space Applications of Automation, Robotics and Machine Intelligence Systems (ARAMIS). Volume 4: Supplement, Appendix 4.3: Candidate ARAMIS Capabilities," NAS 1.26:162083, 1982.

[3] M. De Stefano, H. Mishra, A. M. Giordano, R. Lampariello, and C. Ott, "A Relative Dynamics Formulation for Hardware-in-the-Loop Simulation of On-Orbit Robotic Missions," *IEEE Robotics and Automation Letters*, 2021. DOI: 10.1109/LRA.2021.3064510.

[4] A. Flores-Abad, O. Ma, K. Pham, and S. Ulrich, "A review of space robotics technologies for on-orbit servicing," *Progress in Aerospace Sciences*, 2014. DOI: 10.1016/j.paerosci.2014.03.002.

[5] H. Kolvenbach and K. Wormnes, "Orbit - A Facility for Experiments on Free Floating Contact Dynamics," in *Proceedings ASTRA 2015*, Netherlands: ESA, 2015.

[6] E. Papadopoulos, I. Paraskevas, T. Flessa, K. Nanos, Y. Rekleitis, and I. Kontolatis, "The NTUA Space Robot Simulator: Design & Results," in *10th ESA Workshop on Advanced Space Technologies for Robotics and Automation*, 2008.

[7] J. L. Schwartz, M. A. Peck, and C. D. Hall, "Historical Review of Air-Bearing Spacecraft Simulators," *Journal of Guidance, Control, and Dynamics*, 2003. DOI: 10.2514/2.5085.

[8] M. Leipold, M. Eiden, C. Garner, L. Herbeck, D. Kassing, T. Niederstadt, T. Krüger, G. Pagel, M. Rezazad, H. Rozemeijer, W. Seboldt, C. Schöppinger, C. Sickinger, and W. Unckenbold, "Solar sail technology development and demonstration," *Acta Astronautica*, vol. 52, no. 2-6, pp. 317–326, 2003. DOI: 10.1016/S0094-5765(02)00171-6.

[9] C. Carignan and D. Akin, "The reaction stabilization of on-orbit robots," *IEEE Control Systems Magazine*, 2000. DOI: 10.1109/37.887446.

[10] C. Lotz, Y. Wessarges, J. Hermsdorf, W. Ertmer, and L. Overmeyer, "Novel active driven drop tower facility for microgravity experiments investigating production technologies on the example of substrate-free additive manufacturing," *Advances in Space Research*, vol. 61, no. 8, pp. 1967–1974, 2018. DOI: 10.1016/j.asr.2018.01.010.

[11] C. Menon, A. Aboudan, S. Cocuzza, A. Bulgarelli, and F. Angrilli, "Free-Flying Robot Tested on Parabolic Flights: Kinematic Control," *Journal of Guidance, Control, and Dynamics*, vol. 28, no. 4, pp. 623–630, 2005. DOI: 10.2514/1.8498.

[12] J. F. Lekan, E. S. Neumann, and D. M. Thompson, *Ground-Based Reduced-Gravity Facilities*, 1998.

[13] C. Lotz, B. Piest, E. Rasel, and L. Overmeyer, "The Einstein Elevator: Space Experiments at the new Hannover Center for Microgravity Research," *Europhysics News*, vol. 54, no. 2, pp. 9–11, 2023. DOI: 10.1051/epn/2023201.

[14] X. Ding, Y. Wang, Y. Wang, and K. Xu, "A review of structures, verification, and calibration technologies of space robotic systems for on-orbit servicing," *Science China Technological Sciences*, 2020. DOI: 10.1007/s11431-020-1737-4.

[15] H. Kolvenbach and K. Wormnes, "Recent Developments on On-Orbit, a 3-DOF Free Floating Contact Dynamics Testbed," presented at the 13th International Symposium on Artificial Intelligence, Robotics and Automation in Space (i-SAIRAS 2016), Beijing, China, 2016.

[16] H. Yao, W. Ren, O. Ma, T. Chen, and Z. Zhao, "Understanding the True Dynamics of Space Manipulators from Air-Bearing Based Ground Testing," *Journal of Guidance, Control, and Dynamics*, 2018. DOI: 10.2514/1.g003501.

[17] L. Herbeck, M. Leipold, C. Sickinger, M. Eiden, and W. Unckenbold, "Development and Test of Deployable Ultra-Lightweight CFRP-Booms for a Solar Sail," *Spacecraft Structures, Materials and Mechanical Testing*, ESA Special Publication, vol. 468, C. Stavrinidis, A. Rolfo, and E. Breitbach, Eds., p. 107, 2001.

[18] O. Han, D. Kienholz, P. Janzen, and S. Kidney, "Gravity-Offloading System for Large-Displacement Ground Testing of Spacecraft Mechanisms," 2010.

[19] H. Sawada, K. Ui, M. Mori, H. Yamamoto, R. Hayashi, S. Matunaga, and Y. Ohkami, "Micro-gravity experiment of a space robotic arm using parabolic flight," *Advanced Robotics*, 2004. DOI: 10.1163/15685530432297243 1.

[20] M. Deremetz, M. Debroise, S. Govindaraj, A. But, I. Nieto, M. De Stefano, H. Mishra, B. Brunner, G. Grunwald, M. A. Roa, M. Reiner, M. Závodník, M. Komarek, J. D'Amico, F. Cavenago, J. Gancet, P. Letier, M. Ilzkovitz, L. Gerdes, and M. Zwick, "Demonstrator Design of a modular Multi-Arm Robot for on-orbit large Telescope Assembly," in *Symposium on Advanced Space Technologies in Robotics and Automation*, Noordwijk, Netherlands, 2022.

[21] Brown and J. Dolan, "A Novel Gravity Compensation System for Space Robots," in *Proc. of ASCE Specialty Conference on Robotics for Challenging Environments*, 1994.

[22] L. K. Dungan, P. S. Valle, D. R. Bankieris, A. P. Lieberman, L. Redden, and C. Shy, "Patent: US9194977B1. Active response gravity offload and method," U.S. Patent 9194977B1, 2015.

[23] G. White and Yangsheng Xu, "An active vertical-direction gravity compensation system," *IEEE Transactions on Instrumentation and Measurement*, vol. 43, no. 6, pp. 786–792, 6 Dec./1994. DOI: 10.1109/19.368066.

[24] F. Elhardt, R. Boumann, M. De Stefano, R. Heidel, P. Lemmen, M. Heumos, C. Jeziorek, M. A. Roa, M. Schedl, and T. Bruckmann, "The Motion Suspension System – MSS: A Cable-Driven System for On-Ground Tests of Space Robots," in *Advances in Mechanism and Machine Science*, M. Okada, Ed., vol. 148, Cham: Springer Nature Switzerland, 2023, pp. 379–388. DOI: 10.1007/978-3-031-45770-8_38.

[25] F. Elhardt, R. Boumann, M. De Stefano, R. Heidel, P. Lemmen, M. Heumos, C. Jeziorek, M. A. Roa Garzon, M. Schedl, and T. Bruckmann, "System Requirements Elicitation and Conceptualization for a Novel Space Robot Suspension System," in *17th Symposium on Advanced Space Technologies in Robotics and Automation (ASTRA)*, Leiden, Niederlande, 2023.

[26] R. Heidel, P. Lemmen, R. Boumann, and T. Bruckmann, "Design and implementation of a cable-driven robot for automated masonry of building walls," in *Fachtagung VDI Mechatronik*, Darmstadt: VDI, 2022.

[27] Y. Wu, H. H. Cheng, A. Fingrut, K. Crolla, Y. Yam, and D. Lau, "CU-brick cable-driven robot for automated construction of complex brick structures: From simulation to hardware realisation," in *2018 IEEE International Conference on Simulation, Modeling, and Programming for Autonomous Robots (SIMPAR)*, Brisbane, QLD: IEEE, 2018. DOI: 10.1109/SIMPAR.2018.8376287.

[28] K. Iturralde, M. Feucht, D. Illner, R. Hu, W. Pan, T. Linner, T. Bock, I. Eskudero, M. Rodriguez, J. Gorrotxategi, J. B. Izard, J. Astudillo, J. Cavalcanti Santos, M. Gouttefarde, M. Fabritius, C. Martin, T. Henninge, S. M. Nornes, Y. Jacobsen, A. Pracucci, J. Cañada, J. D. Jimenez-Vicaria, R. Alonso, and L. Elia, "Cable-driven parallel robot for curtain wall module installation," *Automation in Construction*, 2022. DOI: 10.1016/j.autcon.2022.104235.

[29] A. Pott, *Cable-Driven Parallel Robots: Theory and Application* (Springer Tracts in Advanced Robotics). Springer, 2018. DOI: 10.1007/978-3-319-76138-1.

[30] N. Pedemonte, T. Rasheed, D. Marquez-Gamez, P. Long, É. Hocquard, F. Babin, C. Fouché, G. Caverot, A. Girin, and S. Caro, "FASTKIT: A Mobile Cable-Driven Parallel Robot for Logistics," in *Advances in Robotics Research*, ser. Springer Tracts in Advanced Robotics, Cham: Springer International Publishing, 2020, pp. 141–163. DOI: 10.1007/978-3-030-22327-4_8.

[31] M. Harshe, J.-P. Merlet, D. Daney, and S. Bennour, "A Multi-sensors System for Human Motion Measurement: Preliminary Setup," presented at the 13th World Congr. in Mechanism and Machine Science, 2011.

[32] M. Zarebidoki, J. S. Dhupia, and W. Xu, "A Review of Cable-Driven Parallel Robots: Typical Configurations, Analysis Techniques, and Control Methods," *IEEE Robotics & Automation Magazine*, 2022. DOI: 10.1109/MRA.2021.3138387.

[33] M. De Stefano, R. Vijayan, A. Stemmer, F. Elhardt, and C. Ott, "A Gravity Compensation Strategy for On-ground Validation of Orbital Manipulators," in *IEEE Int. Conf. on Robotics and Automation*, London, UK, 2023.

[34] A. Beyer, G. Grunwald, M. Heumos, M. Schedl, R. Bayer, W. Bertleff, B. Brunner, R. Burger, J. Butterfaß, R. Gruber, T. Gumpert, F. Hacker, E. Krämer, M. Maier, S. Moser, J. Reill, M. A. Roa, H.-J. Sedlmayr, N. Seitz, and A. Albu-Schäffer, "CAESAR: Space Robotics Technology for Assembly, Maintenance, and Repair," in *Proc. of the Int. Astronautical Congress*, Bremen, 2018.

[35] P. Letier, T. Siedel, M. Deremetz, E. Pavlovskis, B. Lietaer, K. Nottensteiner, M. A. Roa, J. Sánchez García Casarrubios, J. Romero, and J. Gancet, *HOTDOCK: Design and Validation of a New Generation of Standard Robotic Interface for On-Orbit Servicing*. 2020.

[36] B. Nelson, M. Higashi, and P. Sharp, "Hubble Space Telescope Servicing Mission 3B Media Reference Guide," NASA, 2002.

[37] M. De Stefano, R. Balachandran, and C. Secchi, "A Passivity-Based Approach for Simulating Satellite Dynamics With Robots: Discrete-Time Integration and Time-Delay Compensation," *IEEE Transactions on Robotics*, vol. 36, no. 1, pp. 189–203, 2020. DOI: 10.1109/TRO.2019.2945883.

[38] H. Mishra, A. M. Giordano, M. De Stefano, R. Lampariello, and C. Ott, "Inertia-Decoupled Equations for Hardware-in-the-Loop Simulation of an Orbital Robot with External Forces," in *2020 IEEE/RSJ International Conference on Intelligent Robots and Systems (IROS)*, 2020, pp. 1879–1886. DOI: 10.1109/IROS45743.2020.9341633.

BIOGRAPHY

Ferdinand Elhardt *received his Master's degree in Mechanical Engineering from the Technical University of Munich. He wrote his master's thesis at the Oxford Robotics Institute in the field of robotic locomotion. He joined the Institute of Robotics and Mechatronics at the German Aerospace Center (DLR) in 2021 and is affiliated to the University of Duisburg-Essen. He is responsible for the Motion Suspension System and conducts research on space robot verification and qualification.*

Marco De Stefano *received his bachelor degree in aerospace engineering (2008) and his master's degree cum laude in astronautical engineering (2011) from Sapienza, University of Rome. In 2019, he received his PhD (summa cum laude) from the University of Modena and Reggio Emilia, which was awarded as finalist for the 2020 Georges Giralt PhD Award. Since 2012, he is a researcher with DLR, heading the Flying and Floating-base robot control group since 2023 with main focus on space robot dynamics, control theory, and hardware-in-the-loop simulation.*

Manfred Schedl *received his diploma from the Technical University of Munich. Since 1987, he has been with the Institute of Robotics and Mechatronics at the German Aerospace Center (DLR). He contributed to several space missions, especially ROTEX, ROKVISS, MASCOT and MMX. His experience is in Robotics, Sensor- and Drive-Technology for terrestrial and space applications.*

Martin Stelzer *studied computer science at FH Ingolstadt and the University of Hagen and received his M.Sc. Degree in 2012. Since 2007, he has been working at the German Aerospace Center in the field of onboard software frameworks and was involved in the space projects ROKVISS, Kontur-2, and EROSS IOD.*

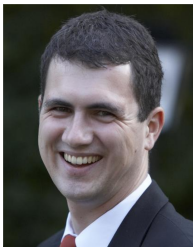

Andreas Stemmer *graduated in Electrical Engineering and Information Technology with major subject Control Theory and Automation Engineering at the Technical University Munich in 2005. He wrote his diploma thesis at the German Aerospace Center (DLR) where he since then works as research engineer. His main fields of interest include software and firmware development as well as joint level control for terrestrial and space robots.*

Ismael Rodriguez *received his degree of Ingeniero en Electrónica from Universidad ORT Uruguay in 2015. In 2023, he received his Ph.D. in Robotics at the Technical University Munich for his research done at the German Aerospace Center (DLR) in Weßling. His research is focused on the development of an assembly planner that is aligned with the requirements of the mass customization phenomenon.*

Ria Vijayan *received her Master's degree in Space Science and Technology from Lulea Technological University, Sweden in 2018. She joined the German Aerospace Center (DLR) in 2021 as a research engineer involved with the space project EROSS IOD among others. Her current doctoral research at DLR, in affiliation with the Technical University of Vienna (TUW), covers robotics, on-orbit servicing, dynamic modeling, nonlinear control, and optimization, with a particular focus on control methods for floating-base robotic systems.*

Tobias Bruckmann *is a senior researcher, lecturer and professor for mechatronics at the University of Duisburg-Essen. His research interests include robotics, automation technology, and human machine interfaces. He has organized and participated in numerous conferences and workshops in the fields of mechatronics and robotics. Tobias Bruckmann has also been involved in several research projects, including the development of a cable-driven parallel robot for use in the construction industry.*

Máximo A. Roa *received his doctoral degree in 2009 from Universitat Politecnica de Catalunya (UPC), and the Project Management Professional (PMP) Certification in 2016. He worked for Hewlett Packard R&D before joining the Institute of Robotics and Mechatronics of the German Aerospace Center (DLR) in 2010 as Senior Research Scientist, leading the group on Robotic Planning and Manipulation.*